Atmos. Meas. Tech., 8, 4817–4830, 2015
www.atmos-meas-tech.net/8/4817/2015/
doi:10.5194/amt-8-4817-2015

Atmospheric Measurement Techniques
Open Access
EGU

Simulated retrievals for the remote sensing of CO_2, CH_4, CO, and H_2O from geostationary orbit

X. Xi[1], V. Natraj[2], R. L. Shia[1], M. Luo[2], Q. Zhang[1], S. Newman[1], S. P. Sander[2], and Y. L. Yung[1,2]

[1]Environmental Science and Engineering, California Institute of Technology, Pasadena, California, USA
[2]Jet Propulsion Laboratory, California Institute of Technology, Pasadena, California, USA

Correspondence to: X. Xi (xixi@caltech.edu)

Received: 21 April 2015 – Published in Atmos. Meas. Tech. Discuss.: 12 June 2015
Revised: 3 September 2015 – Accepted: 5 October 2015 – Published: 18 November 2015

Abstract. The Geostationary Fourier Transform Spectrometer (GeoFTS) is designed to measure high-resolution spectra of reflected sunlight in three near-infrared bands centered around 0.76, 1.6, and 2.3 µm and to deliver simultaneous retrievals of column-averaged dry air mole fractions of CO_2, CH_4, CO, and H_2O (denoted XCO_2, XCH_4, XCO, and XH_2O, respectively) at different times of day over North America. In this study, we perform radiative transfer simulations over both clear-sky and all-sky scenes expected to be observed by GeoFTS and estimate the prospective performance of retrievals based on results from Bayesian error analysis and characterization.

We find that, for simulated clear-sky retrievals, the average retrieval biases and single-measurement precisions are < 0.2 % for XCO_2, XCH_4, and XH_2O, and < 2 % for XCO, when the a priori values have a bias of 3 % and an uncertainty of 3 %. In addition, an increase in the amount of aerosols and ice clouds leads to a notable increase in the retrieval biases and slight worsening of the retrieval precisions. Furthermore, retrieval precision is a strong function of signal-to-noise ratio and spectral resolution. This simulation study can help guide decisions on the design of the GeoFTS observing system, which can result in cost-effective measurement strategies while achieving satisfactory levels of retrieval precisions and biases. The simultaneous retrievals at different times of day will be important for more accurate estimation of carbon sources and sinks on fine spatiotemporal scales and for studies related to the atmospheric component of the water cycle.

1 Introduction

The global carbon cycle has been significantly perturbed since the start of industrialization. The atmospheric concentrations of the greenhouse gases (GHG) carbon dioxide (CO_2), methane (CH_4), and the pollutant carbon monoxide (CO) have all increased substantially due to anthropogenic activities (IPCC, 2013). These potent greenhouse gases trap outgoing long-wave radiation and warm the Earth's atmosphere and surface. As surface temperature continues to rise, the global water cycle is also notably changed (IPCC, 2013). Being the most potent greenhouse gas, water vapor (H_2O) is of crucial importance to climate studies. An accurate understanding of carbon storage in the atmosphere, oceans, and terrestrial biosphere, as well as the exchanges between these reservoirs and the coupling with the water cycle, is critical to confidently project the future evolution of climate and to support societal efforts to mitigate climate change. However, despite decades of research, the Earth's carbon budget, especially the changes in the carbon sinks, still remains uncertain on regional and global scales (Le Quéré et al., 2009, 2014). In particular, two major challenges remain in balancing the carbon budget: quantifying uncertainty in fossil fuel CO_2 emissions (Le Quéré et al., 2009), and constraining the variability and uncertainty of land fluxes (Schimel et al., 2001; Houghton et al., 2007).

To tackle these challenges in carbon cycle studies, several satellite missions have been measuring the atmospheric concentrations of greenhouse gases such as CO_2 and CH_4. For example, the Atmospheric Infrared Sounder (AIRS), whose main scientific goal is to improve weather forecasting, has been able to measure mid-tropospheric CO_2 and CH_4 since

2002 (Aumann et al., 2003; Chahine et al., 2005, 2008; Xiong et al., 2008). The Scanning Imaging Absorption Spectrometer for Atmospheric Cartography (SCIAMACHY) instrument was operational for measurements of atmospheric compositions from 2002 to 2012, with CO_2, CH_4, CO, and H_2O as four of its target species (Buchwitz et al., 2004, 2007; Schrijver et al., 2009; Schneising et al., 2011). The Greenhouse gases Observing SATellite (GOSAT), developed by the Japan Aerospace Exploration Agency and launched in January 2009, is the world's first mission dedicated to the monitoring of CO_2 and CH_4 (Yokota et al., 2009; Butz et al., 2011; Yoshida et al., 2011). In addition, the Orbiting Carbon Observatory (OCO)-2 mission, successfully launched in July 2014, now provides high-quality and worldwide column abundances of CO_2 (Crisp et al., 2004, 2012).

Flying in a low Earth orbit (LEO), these missions can achieve nearly global coverage in about 16 days and offer monthly averaged retrievals of greenhouse gases. One exception is SCIAMACHY that had a revisit time of 6 days. The sources and sinks of greenhouse gases are then inferred through flux inversions (e.g., Baker et al., 2010; Nassar et al., 2011). However, the low spatiotemporal measurement densities of the current Earth observing system in LEO result in a lack of information about emissions on smaller spatiotemporal scales (Chevallier et al., 2005; Hungershoefer et al., 2010; Wecht et al., 2014). For example, localized emissions from forest fires and megacities vary over days or even hours. Furthermore, as the carbon and water cycles are closely coupled in the terrestrial biosphere, there is a significant scientific need to simultaneously study both on a daily basis.

The Geostationary Fourier Transform Spectrometer (GeoFTS) combines an imaging Fourier transform spectrometer instrument with a geostationary Earth orbit vantage point and thereby promises to realize a transformational advance in carbon and water monitoring beyond the synoptic capability of the current LEO instruments. As a proposed mission at this point in time, it is designed to measure high-resolution spectra of reflected sunlight in near-infrared bands and to deliver simultaneous retrievals of column-averaged dry air mole fractions of CO_2, CH_4, CO, and H_2O (denoted XCO_2, XCH_4, XCO, and XH_2O, respectively) at different times of day over North America. A prototype of the instrument on top of Mount Wilson, in the San Gabriel Mountains just north of Los Angeles, California, has been collecting high-quality data over that megacity since August 2011 (Key et al., 2012; Fu et al., 2014; Wong et al., 2015). The main scientific objectives of GeoFTS are the following:

1. to provide observations with the spatial and temporal density required to enable reliable flux inversions, which allow assessments of surface-atmosphere carbon exchange on scales that mirror fundamental carbon cycle processes; to better constrain the flux inversions, the requirements for single-sounding XCO_2, XCH_4, and XCO retrieval precisions are less than 0.5 % ($\sim$ 2 ppmv), 1 % ($\sim$ 18 ppbv), and 10 % ($\sim$ 12 ppbv), respectively (Rayner et al., 2001, 2014);

2. to quantify the magnitude and spatiotemporal patterns of atmospheric signatures of anthropogenic CO_2, CH_4, and CO emissions (e.g., Newman et al., 2013);

3. to use the retrievals of XH_2O to monitor the atmospheric component of the water cycle. Because water vapor is the dominant greenhouse gas and its amount in the atmosphere is controlled by temperature, it constitutes a positive feedback on climate (Bengtsson, 2010) and needs to be monitored on a fine spatiotemporal scale.

Simulation studies have been done in the past to evaluate the design of proposed observing systems and have proven to be informative for the design of new missions. For example, Kuang et al. (2002) conducted an introductory study on the potential of using a 3-band spectrometric approach to accurately measure atmospheric CO_2 from space. The OCO-2 mission has adopted the measurement strategy pioneered by their simulation study. Buchwitz et al. (2013) developed an error parameterization scheme for the proposed CarbonSat mission and assessed atmospheric CO_2 and CH_4 retrieval errors in a simulated environment. Polonsky et al. (2014) conducted end-to-end simulated retrievals for the proposed geoCARB mission and found that accurate measurements of trace gases make it possible to monitor localized emission sources such as power plants.

In this study, we perform radiative transfer simulations over both clear-sky and all-sky scenes expected to be observed by GeoFTS and estimate the prospective performance of retrievals based on results from Bayesian error analysis and characterization. This paper is structured as follows. Section 2 explains the methodology of simulated retrievals. Section 3 presents and discusses the results of column-averaged retrievals, their sensitivity to signal-to-noise ratio (SNR) and spectral resolution, and the influence of aerosols and clouds. Section 4 summarizes the major scientific contributions and some limitations of this study.

2 Methodology

This section presents the design of the observing system for GeoFTS, the set-up for the simulated retrievals, the forward model, the retrieval algorithm, and some diagnostics of the observing system.

2.1 Design of the GeoFTS observing system

The science objectives of GeoFTS require continuous coverage of bioactive land surfaces, as well as major population centers. It will cover the latitude range of 60° N to 60° S based on an assumed 95° W geostationary longitude. For

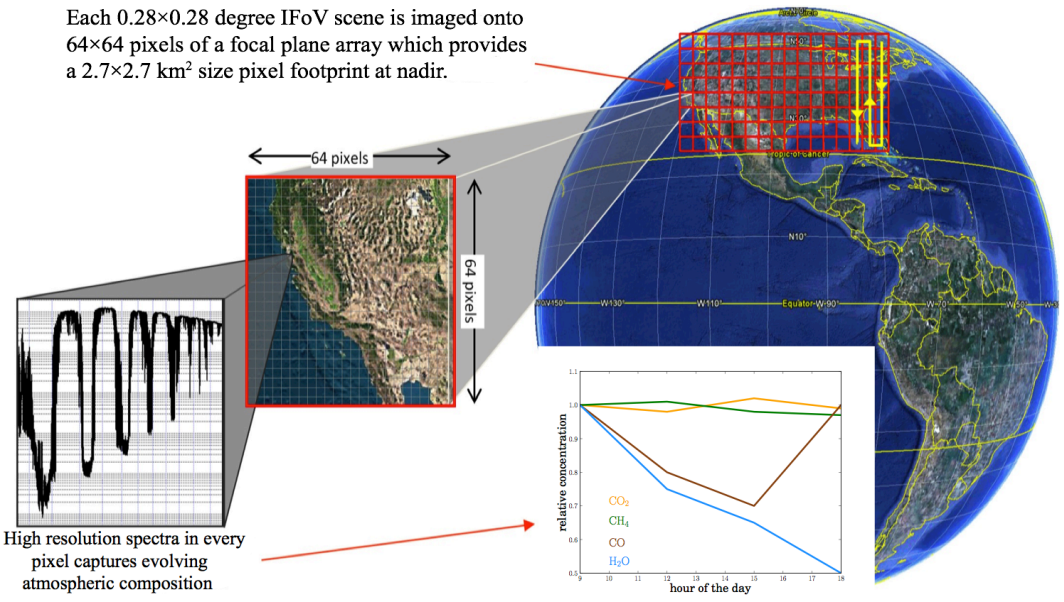

Figure 1. A schematic illustrating the GeoFTS observing system. Each $0.28 \times 0.28°$ instantaneous field of view (IFoV) scene is imaged onto 64×64 pixels of a focal plane array, which provides a $2.7 \times 2.7\,km^2$ size pixel footprint at nadir. The evolving atmospheric compositions at different times of day (LT) are then inferred from the high-resolution spectra measured by the instrument. The relative concentrations of four target species with respect to those at 9 a.m. are shown for illustration purposes only.

the purposes of this study, we focus only on North America from 60 to 30° N. Figure 1 shows a schematic diagram of the GeoFTS observing system. At a fixed position relative to Earth, an FTS (Fourier transform spectrometer) with agile pointing optics can scan all of North America in any pattern. The spatial resolution is designed to match modeling scales: 10 km for urban models and 10–50 km for regional flux inversion models. In addition, to maximize the fraction of clear-sky scenes, small footprints are needed. In GeoFTS, each $0.28 \times 0.28°$ instantaneous field of view (IFoV) scene is imaged onto 64×64 pixels of a focal plane array, which provides a $2.7 \times 2.7\,km^2$ size pixel footprint at nadir. The evolving atmospheric compositions are then inferred from the high-resolution spectra measured by the instrument. Fu et al. (2014) provide more details about a prototype of the instrument on Mount Wilson. The real instrument in space will be similar to the prototype, although the viewing geometry and the spectral resolution will be different from those for the ground-based instrument.

For flux modeling, the temporal resolution needs to be paired to regional flux models, which use 1 to 6 h time steps and estimate daily fluxes (Wu et al., 2011). Considering that about 20–30 % of the scenes over North America are without excessive aerosol and cloud loadings (Bréon et al., 2005), and taking into account the time steps used in flux models, at least four revisits per day are required. This revisit frequency requires GeoFTS to scan all of North America in about 3 hours when there is sufficient reflected sunlight to be measured. This will result in at most four useful measurements each day, thus capturing the diurnal variations of trace gases. An integration time of about 1 minute for each footprint should give a SNR of about 300. The scanning pattern shown in Fig. 1 is one of the many possible options available for GeoFTS. Faster revisit intervals are possible but involve trade-offs between SNR, spatial resolution, and geographic coverage.

Three spectral bands are chosen to meet the GeoFTS science objectives. Table 1 shows the spectral bands used and the target species in each band. Band 1A is used for retrievals of CH_4, CO, and H_2O and Band 1B for CH_4, CO_2, and H_2O. Band 2 is the O_2 A-band, which provides information about surface pressure, aerosols, and clouds (Crisp et al., 2004).

2.2 Set-up for simulated retrievals

After designing the observing system, studies need to be performed to evaluate whether this specific design will meet the requirements for single-sounding XCO_2, XCH_4, and XCO retrieval precisions. This is done through simulated retrievals, as illustrated in Fig. 2. We use realistic atmospheric profiles from the GEOS-CHEM global 3-D chemical transport model (Bey et al., 2001), with line positions and strengths obtained from the HITRAN 2008 molecular spectroscopic database. These are then input to a line-by-line radiative transfer model (LBLRTM) (Clough et al., 2005) to generate the optical depths (ODs). The state-of-the-art vector linearized discrete ordinate radiative transfer (VLIDORT) model (Spurr, 2006) generates the synthetic radiance data after its model output is convolved with the instrument line

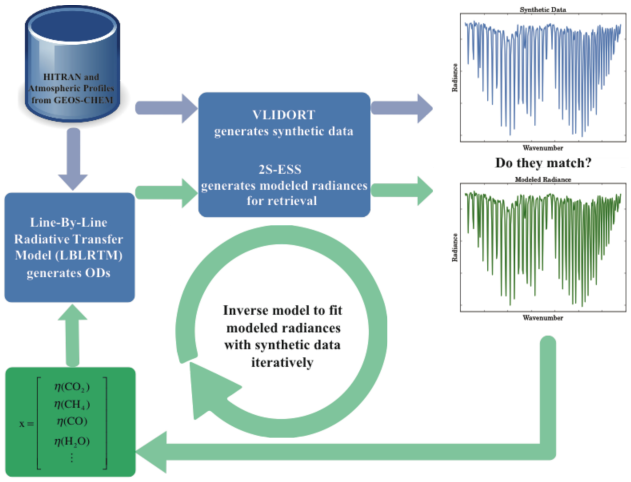

Figure 2. The set-up for simulated retrievals. Realistic atmospheric profiles are obtained from GEOS-CHEM and line positions and strengths from the HITRAN 2008 molecular spectroscopic database. These are then input to a line-by-line radiative transfer model (LBLRTM) to generate optical depths. VLIDORT, a state-of-the-art radiative transfer model, generates the synthetic data after its model output is convolved with the instrument line shape (ILS) and random measurement noise is added. A fast two-stream (2S), enhanced single scattering (ESS) radiative transfer model, 2S-ESS, generates the modeled radiances for retrievals. In simulated retrievals, we first have some prior knowledge about the concentration of gases and other parameters. This a priori is used as input to 2S-ESS to generate the modeled radiances. The state vector $\boldsymbol{x}$ is updated iteratively in an inverse model until the modeled radiances match the synthetic data adequately.

shape (ILS) and white Gaussian measurement noise is added. A combination of a two-stream (2S) multiple scattering and an exact single scattering (ESS) model, henceforth referred to as the 2S-ESS model, generates the modeled radiances for the retrieval. The 2S-ESS model also accounts for scattering effects of aerosols and clouds (Spurr and Natraj, 2011; Natraj, 2013), albeit not as accurately as VLIDORT. The differences between the VLIDORT and 2S-ESS models give a conservative representation of the forward model error in real retrievals.

The atmospheric profile used to generate the synthetic data is regarded as the "truth". In retrievals where we do not know the "truth", we first have some prior knowledge about the concentration of gases in the air column, $\boldsymbol{x}_a$. This a priori is used as input to the LBLRTM and 2S-ESS models to generate the modeled radiances. The state vector $\boldsymbol{x}$ is updated iteratively until the modeled radiances match the synthetic data adequately. If and when the two spectra do match, the state vector $\boldsymbol{x}$ is then called the "retrieved" state.

Ten test locations in North America are chosen over a significant range of latitudes and longitudes on 26 and 30 July 2006. These 2 days are a Wednesday and a Sunday, respectively, thus accounting for the weekday–weekend variations

Table 1. The GeoFTS spectral bands and the target species.

Band Number	Spectral band	Target species
1A	2.3 µm (4210–4320 cm^{-1})	CH_4, CO, H_2O
1B	1.6 µm (5950–6100 and 6190–6260 cm^{-1})	CH_4, CO_2, H_2O
2	0.76 µm (13 000–13 170 cm^{-1})	O_2

in anthropogenic emissions. We will show specific results from Location 1 in Central California and retrieval statistics based on all 10 locations. The original 116-level atmospheric profiles from the GEOS-CHEM model are interpolated to 20 carefully chosen levels. The Solar Irradiance Reference Spectra (SIRS) (Woods et al., 2009) is linearly interpolated to the wave numbers in the GeoFTS spectral bands. For simplicity, surface reflection is assumed to be Lambertian. Broadband surface emissivity for each location is obtained from spaceborne measurements (Jacob et al., 2004).

2.2.1 Forward model

In case of space-borne remote sensing observations of the atmospheric composition, a forward model translates the concentration of gases in the atmosphere to the upwelling radiances measured by an instrument in space. In this study, there are two components to the forward model. The first component is the LBLRTM model that takes in an atmospheric profile and computes the ODs of each gaseous species based on spectroscopic information in the HITRAN 2008 database (Rothman et al., 2009). The absorption cross section (σ) from the LBLRTM, the concentration of the gaseous species ($[C]$) at various atmospheric heights (z), and the total column-integrated OD of the gas (τ) are related as follows:

$$\tau = \int_0^\infty \sigma \cdot [C] \mathrm{d}z. \quad (1)$$

Figure 3 shows the ODs of the four target species. CO_2, CH_4, and H_2O absorb strongly in these spectral bands. Although CO only absorbs weakly, its absorption strength is sufficient for good retrievals in clear-sky conditions, as will be shown in Sect. 3.1. For all-sky retrievals, four types of aerosols (black carbon, organic carbon, sea salt, and sulphate) with realistic vertical profiles and diurnal variations are taken from GEOS-CHEM model output and introduced into the model atmosphere. Based on cloud observations from the CALIPSO mission (Winker et al., 2010), we also introduce a small amount of ice clouds to regions near the tropopause. The optical properties of both aerosols and ice clouds are calculated using Mie theory with parameterized Gamma particle size distributions (Heymsfield et al., 2002).

The second component of the forward model is the radiative transfer model (VLIDORT for generating synthetic data

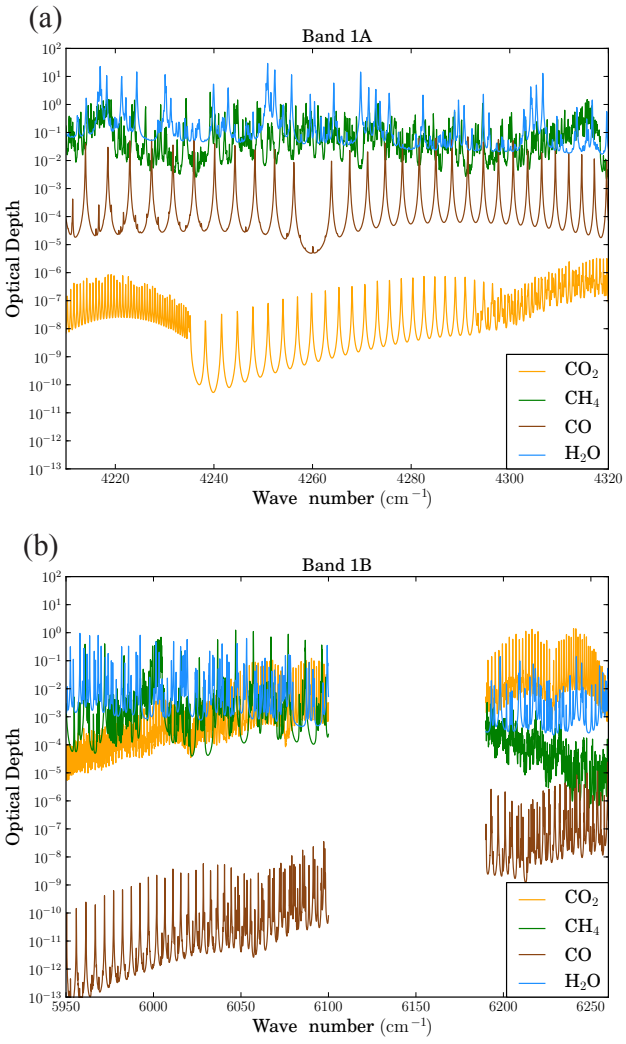

Figure 3. The optical depths of four target species in the GeoFTS spectral bands: **(a)** for Band 1A and **(b)** for Band 1B. Band 1A is for retrievals of CH_4, CO, and H_2O. Band 1B is for retrievals of CH_4, CO_2, and H_2O.

and 2S-ESS for retrieval). Both models take in the same optical depths of all the absorbing and scattering species (GHG, aerosols, and ice clouds) and compute the upwelling radiances based on the viewing geometry, the solar irradiance, and other auxiliary parameters. The zenith and azimuth angles of the Sun and the satellite are computed for each location at different times of day. The main difference between the two models is the better characterization of the scattering effects of aerosols and clouds in VLIDORT. This comprehensive radiative transfer model can use any number of computational quadrature angles ("streams") for the discrete ordinates calculation and we employ 16 streams in our calculations. Both models are run with a spectral resolution of 0.05 cm^{-1}. Then, these high-resolution spectra are convolved with the GeoFTS ILS function to produce low-resolution spectra (0.25 cm^{-1}) (see Fig. 2 of Fu et al., 2014 for the ILS). The radiances generated from VLIDORT, with measurement noise added in, mimic the measurements that GeoFTS would make from the geostationary orbit. The outputs from 2S-ESS are the modeled radiances used in retrievals and they do not contain any measurement noise. Initially, the SNR is set at 300 and the spectral resolution at 0.25 cm^{-1}. These two parameters can be changed in the actual design of the observing system. The choices of SNR and spectral resolution and their impact on the retrieval results are discussed in Sect. 3.3.

Several assumptions have been made in the forward model. It has been assumed that the spectroscopic parameters and the ILS are known with certainty and the surface is Lambertian. In reality, uncertainties in these variables would lead to retrieval errors (e.g., Wunch et al., 2011; Fu et al., 2014). In addition, no micro-windows are used in this study. They could be selected in the future to alleviate the problem of interference among the retrieved parameters and to speed up the numerical computations (e.g., Rodgers, 1998; Vidot et al., 2009; Kuai et al., 2010).

2.2.2 Retrieval algorithm

We use a non-linear Maximum A Posteriori (MAP) method to iteratively retrieve the state vector $\boldsymbol{x}$ (Rodgers, 2000). This method for retrieval has been widely used for GOSAT (Yoshida et al., 2011), Tropospheric Emission Spectrometer, and OCO-2 (Kuang et al., 2002; Connor et al., 2008; O'Dell et al., 2012; Crisp et al., 2012). The state vector $\boldsymbol{x}$, model parameters $\boldsymbol{b}$, and error $\boldsymbol{e}$ are related to the measurement vector $\boldsymbol{y}$ by a forward model $\mathbf{F}$:

$$\boldsymbol{y} = \mathbf{F}(\boldsymbol{x}, \boldsymbol{b}) + \boldsymbol{e}. \tag{2}$$

The model parameters include trace gas spectroscopy and geometric and optical properties of aerosols and clouds. The errors include both the forward model error and the instrument noise. The goal of the non-linear MAP method is to minimize the Bayesian least-squares cost function, which is defined as follows:

$$J(\boldsymbol{x}) = [\boldsymbol{y} - \mathbf{F}(\boldsymbol{x}, \boldsymbol{b})]^{\mathrm{T}} \mathbf{S}_{\mathrm{e}}^{-1} [\boldsymbol{y} - \mathbf{F}(\boldsymbol{x}, \boldsymbol{b})] + (\boldsymbol{x} - \boldsymbol{x}_{\mathrm{a}})^{\mathrm{T}} \mathbf{S}_{\mathrm{a}}^{-1} (\boldsymbol{x} - \boldsymbol{x}_{\mathrm{a}}). \tag{3}$$

$\mathbf{S}_{\mathrm{a}}$ and $\mathbf{S}_{\mathrm{e}}$ are the error covariance matrices for the a priori and the measurement, respectively. $\mathbf{S}_{\mathrm{e}}$ is assumed to be a diagonal matrix with values of the square of the noise. $\boldsymbol{x}$ and $\boldsymbol{x}_{\mathrm{a}}$ are the true state and the a priori, respectively. The Levenberg-Marquardt method (Levenberg, 1944; Marquardt, 1963) is used to obtain stable retrieval results within a trust region for nonlinear least-squares problems. In each iteration, the $(i+1)$th state vector, $\boldsymbol{x}_{i+1}$, is related to the ith state vector, $\boldsymbol{x}_i$, as follows:

$$\boldsymbol{x}_{i+1} = \boldsymbol{x}_i + [(1+\gamma)\mathbf{S}_\mathrm{a}^{-1} + \mathbf{K}_i^\mathrm{T}\mathbf{S}_\mathrm{e}^{-1}\mathbf{K}_i]^{-1}\mathbf{K}_i^\mathrm{T}\mathbf{S}_\mathrm{e}^{-1} \left[\boldsymbol{y} - \mathbf{F}(\boldsymbol{x}_i)\right] - \mathbf{S}_\mathrm{a}^{-1}[\boldsymbol{x}_i - \boldsymbol{x}_\mathrm{a}]\}. \quad (4)$$

The parameter γ is set at 10 initially and updated after each iteration. $\mathbf{F}(\boldsymbol{x}_i)$ is the forward model output based on the state vector $\boldsymbol{x}_i$. $\mathbf{K}_i$ $(\delta\mathbf{F}(\boldsymbol{x}_i)/\delta\boldsymbol{x}_i)$ is a Jacobian matrix that describes how the modeled radiances change given an infinitesimal change in $\boldsymbol{x}_i$. It is computed using the finite difference method. The iterations stop when each element of $\boldsymbol{x}_{i+1}$ differs from the corresponding one in $\boldsymbol{x}_i$ by less than 0.001. Typically, it takes 5–10 iterations for retrievals to converge on stable results. Since this study is meant to serve as a proof of concept, the state vector is slightly simpler than that anticipated to be used in the real retrievals. The state vector is defined in the following way:

$$\boldsymbol{x} = \begin{bmatrix} \eta(\mathrm{CO_2}) \\ \eta(\mathrm{CH_4}) \\ \eta(\mathrm{CO}) \\ \eta(\mathrm{H_2O}) \\ \eta(T) \\ \eta(p) \\ \eta(\varepsilon) \\ \eta(\mathrm{fs}) \\ \eta(\mathrm{zo}) \end{bmatrix} \quad \text{for total column retrieval in clear sky conditions.} \quad (5)$$

Here η stands for the multiplicative scaling factor retrieved for the atmospheric profile and other parameters (T: temperature profile; p: pressure profile; ε: broadband surface emissivity; fs: frequency shift; zo: zero-level offset). As surface albedo is equal to 1 minus surface emissivity and varies from site to site, by retrieving a scaling factor for surface emissivity, we retrieve surface albedo indirectly. For each element in the state vector, the a priori is biased 3 % with respect to the true state, so as to allow easy comparison among retrieved values. The a priori one-sigma (1σ) error is also set at 3 %, thus providing a fairly loose constraint on the a priori and making the retrieval dependent on the measurement rather than the prior knowledge. Note that the a priori constraints are small compared to the true uncertainties of XH_2O and XCO. More realistic a priori values will be used in operational retrievals. For this simulation study, we choose to set all of the a priori biases and errors to 3 % so as to compare the retrieval results for all four target species. All the elements are assumed to be independent of each other; i.e., $\mathbf{S}_\mathrm{a}$ is diagonal. The retrieved state vector can be expressed as

$$\hat{\boldsymbol{x}} = \mathbf{A}\boldsymbol{x} + (\mathbf{I}_n - \mathbf{A})\,\boldsymbol{x}_\mathrm{a} + \mathbf{G}\boldsymbol{e}. \quad (6)$$

The first term on the right hand side, $\mathbf{A}\boldsymbol{x}$, represents the contribution of the true state to the retrieved state. The averaging kernel $\mathbf{A}$ is defined as

$$\mathbf{A} = \frac{\partial\hat{\boldsymbol{x}}}{\partial\boldsymbol{x}} = (\mathbf{K}^\mathrm{T}\mathbf{S}_\mathrm{e}^{-1}\mathbf{K} + \mathbf{S}_\mathrm{a}^{-1})^{-1}\mathbf{K}^\mathrm{T}\mathbf{S}_\mathrm{e}^{-1}\mathbf{K} = \mathbf{G}\mathbf{K}. \quad (7)$$

It quantifies the relative contribution to the retrieval from the true state, compared to that from the a priori. Correspondingly, $(\mathbf{I}_n - \mathbf{A})$ represents the relative contribution to the retrieval from the a priori. The second term, $(\mathbf{I}_n - \mathbf{A})\boldsymbol{x}_\mathrm{a}$, is also known as the smoothing error because it smoothes the solution towards the a priori. In the third term, $\mathbf{G}$ stands for the gain matrix and $\mathbf{G}\boldsymbol{e}$ represents the retrieval error due to the random instrument noise and the forward model error. The error covariance matrix for the retrieved state, $\hat{\mathbf{S}}$, quantifies the uncertainties in the retrieval based on $\mathbf{S}_\mathrm{a}$, $\mathbf{S}_\mathrm{e}$, and $\mathbf{K}$:

$$\hat{\mathbf{S}} = (\mathbf{K}^\mathrm{T}\mathbf{S}_\mathrm{e}^{-1}\mathbf{K} + \mathbf{S}_\mathrm{a}^{-1})^{-1}. \quad (8)$$

The square roots of its diagonal values give the 1σ uncertainty of the retrievals.

2.3 Diagnostics of the observing system

In order to examine whether the design of the GeoFTS observing system would result in precise trace gas retrievals, we implement the following diagnostics (Rodgers, 2000).

- Jacobian ($\mathbf{K}$): the sensitivity of the modeled radiances to the state vector. A large Jacobian indicates that a gaseous species absorbs strongly in the spectral band.
- Averaging kernel ($\mathbf{A}$): quantifies the relative contribution to the retrieval from the true state, compared to that from the a priori. Ideally, it should be close to unity.
- Degrees of freedom for signal (DoF): describes the number of useful independent quantities there are in a measurement. DoF = trace($\mathbf{A}$).
- Information content (H): quantitatively describes how well the measurements increase our confidence in the estimation of the atmospheric state relative to the prior knowledge. As a scalar quantity, H is useful for characterizing and comparing observing systems. Mathematically, it is defined as

$$H = \frac{1}{2}\ln(\left|\hat{\mathbf{S}}^{-1}\mathbf{S}_\mathrm{a}\right|). \quad (9)$$

- Retrieval bias: defined as the absolute percentage difference between the retrieval and the truth.
- Single-measurement precision: the 1σ uncertainty of the retrieval σ_p, where p stands for the posterior state.
- Uncertainty reduction (UR): defined as $(\sigma_\mathrm{a} - \sigma_\mathrm{p})/\sigma_\mathrm{a} \times 100\,\%$, where σ_a and σ_p stand for uncertainty of the a priori and the a posteriori, respectively.

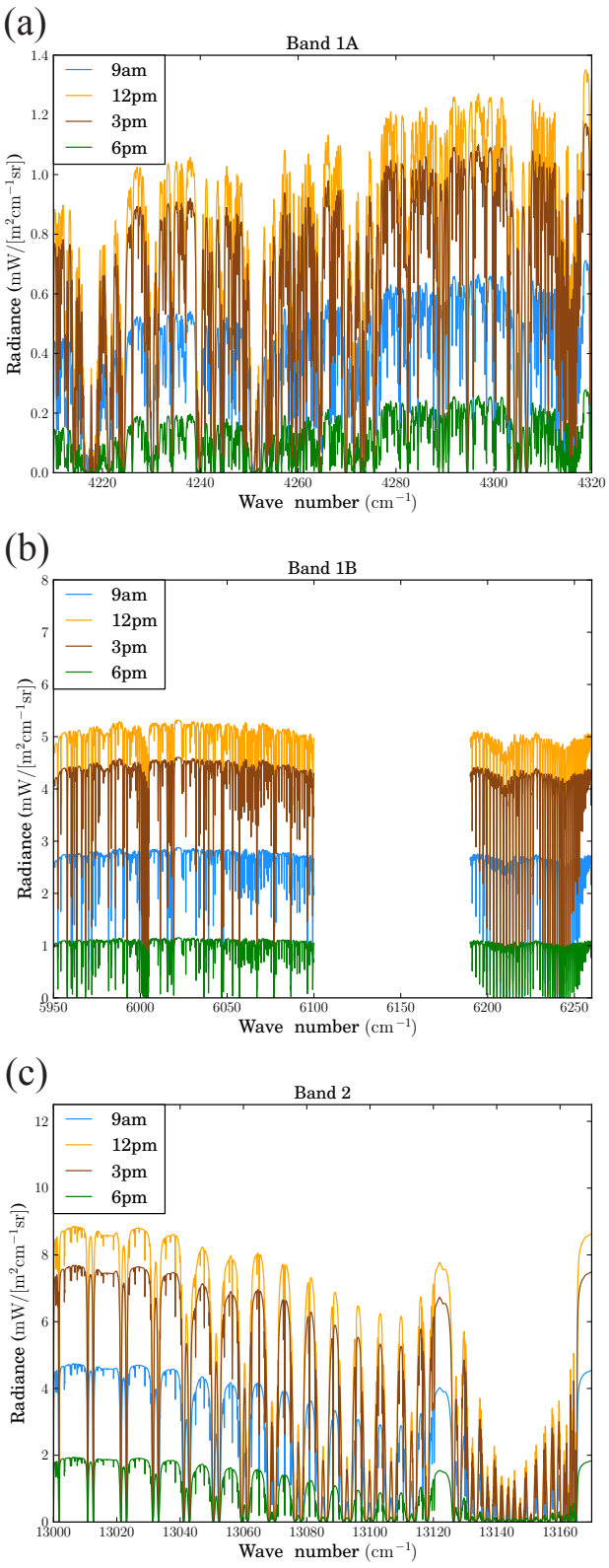

Figure 4. Modeled radiances in three spectral bands at four times of day at Location 1 on 26 July 2006.

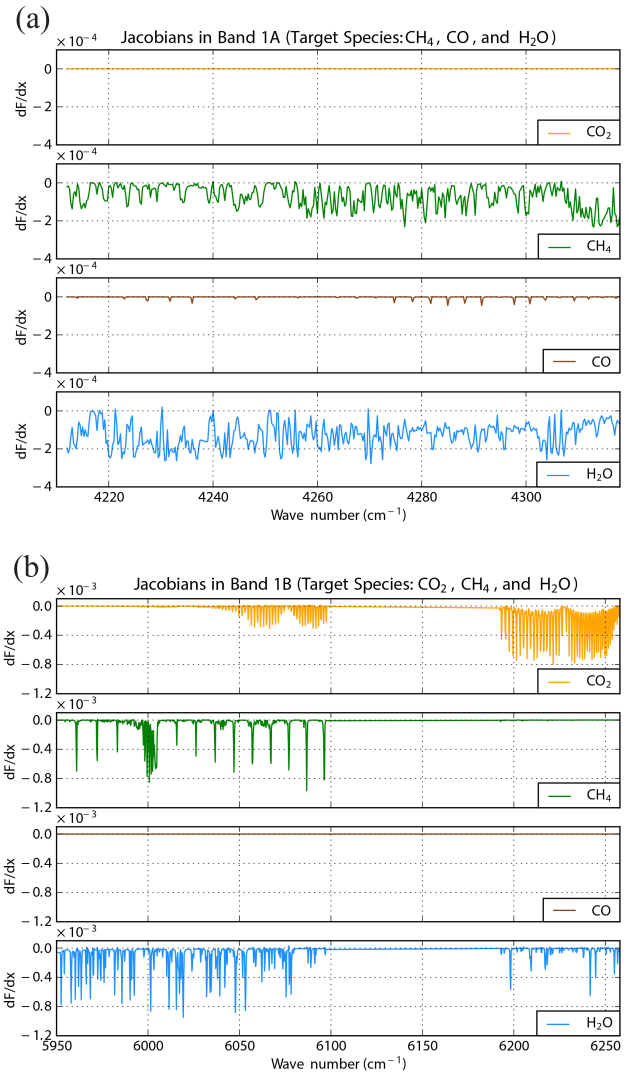

Figure 5. The Jacobians of four target species in **(a)** Band 1A and **(b)** Band 1B. Since x is a unitless scaling factor, the Jacobian ($\mathrm{d}F/\mathrm{d}x$) has the same unit as the modeled radiances in Fig. 4.

3 Results and discussion

3.1 Simulated retrievals in clear sky conditions

For clear-sky retrievals, the forward model generates the upwelling radiances based on the trace gas atmospheric profiles and other auxiliary parameters. Figure 4 illustrates the modeled radiances at four times of day at Location 1, a test location in Central California. As expected, the reflected sunlight captured by GeoFTS will be more intense at 12 and 3 p.m. and less so at 9 a.m. and 6 p.m. The times here refer to the local time (LT). This indicates that radiative transfer models dedicated to geostationary measurements can realistically simulate the diurnal variations of radiances.

Figure 5 shows the Jacobians for the four target species. CO_2, CH_4, and H_2O absorb strongly in the two bands, while

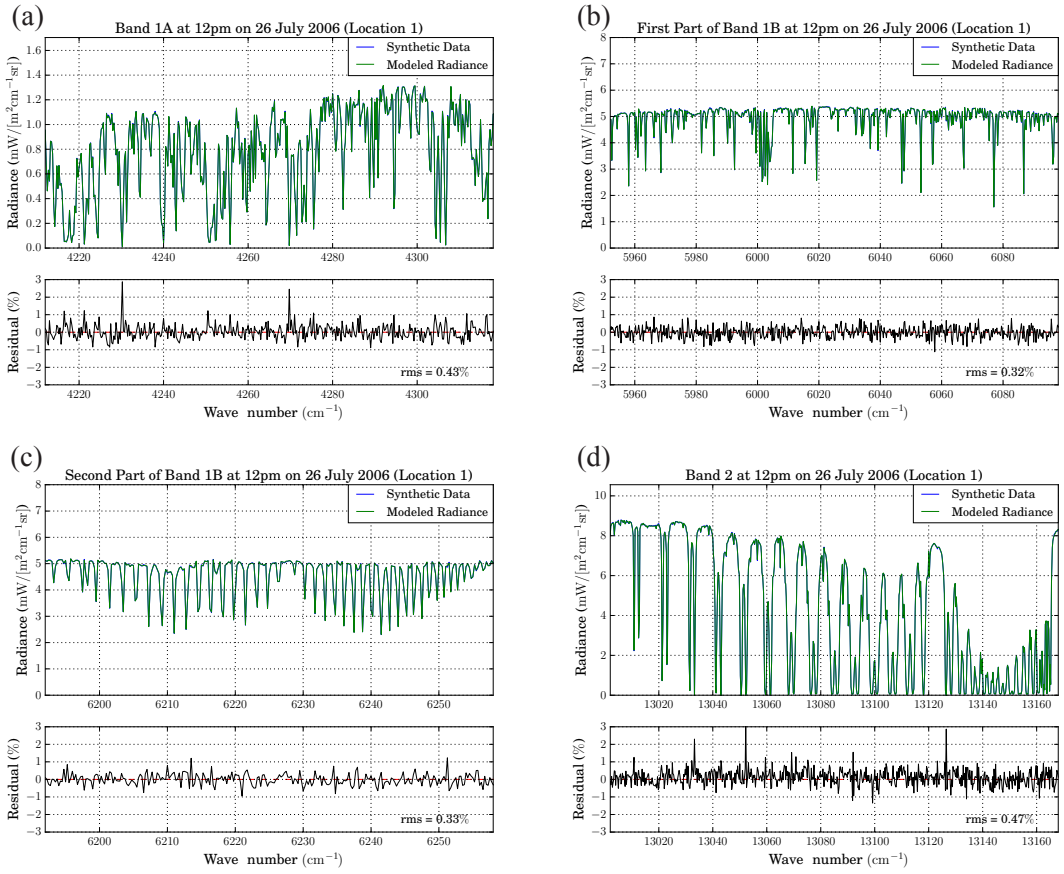

Figure 6. A sample spectral fit and residuals from a simulated clear-sky retrieval on 26 July 2006 at Location 1. The root-mean-square (rms) values of the residuals are between 0.32 and 0.47 %.

the CO absorptions are much weaker. The relative absorption strengths suggest that the retrieval results are likely to be better for CO_2, CH_4, and H_2O. Through the iterative retrieval algorithm, a fit is obtained between the modeled radiances and the synthetic data. Figure 6 shows a sample spectral fit and residuals in all spectral bands. The fact that the residuals fluctuate randomly around zero and follow an approximate Gaussian distribution (not shown) indicates that most of the information from the spectra has been extracted. Minor inaccuracies in the retrieved state result in some small spikes in the residuals. If the forward model is perfect and the SNR is 300, the theoretical lower limit for the root-mean-square (rms) value of the residuals is approximately 0.33 %. The real rms values of the residuals from this simulated retrieval are close to the theoretical value, implying that most of the residuals are due to the random instrument noise, and not the forward model error.

The averaging kernel approaches a unitary matrix (not shown). This indicates that most of the elements in the retrieved state are sensitive to the true state. Since the state vector for clear-sky retrievals contains 9 elements, as shown in Eq. (5), the theoretical upper limit for DoF is 9. Through simulated retrievals, the real DoF is calculated to be around 8.7. It falls slightly short of 9 because of the relatively weak absorption of CO. The information content is around 42. This validates our expectation that the spectral measurements significantly improve our knowledge of the atmospheric state.

Figure 7 summarizes the statistics of the retrieval results at 10 locations over the 2 test days. There are a total of 10 (locations) $\times$ 2 (days) $\times$ 4 (times of day) $=$ 80 test cases and there is one simulated retrieval for each test case. The error bars show the standard deviations of the results over the 10 locations. Most of the retrievals are highly accurate and precise in clear-sky conditions. The average retrieval biases and single-measurement precisions are <0.2 % for XCO_2, XCH_4, and XH_2O, and <2 % for XCO. The retrieval results for XCO_2 and XCH_4 are comparable to simulated retrievals by Polonsky et al. (2014), which examined XCO_2, XCH_4, and XCO retrievals using similar spectral bands and the OCO simulator. The biases in XCO retrievals in their study are larger than the results presented here. This is mainly due to different smoothing errors based on different a priori values. As expected, our simulation results show smaller biases and better precisions than those in real retrievals (e.g., Fu et al., 2014; Crisp et al., 2012), partly because of the assumptions discussed in Sect. 2.2.1 and the different spectral bands used.

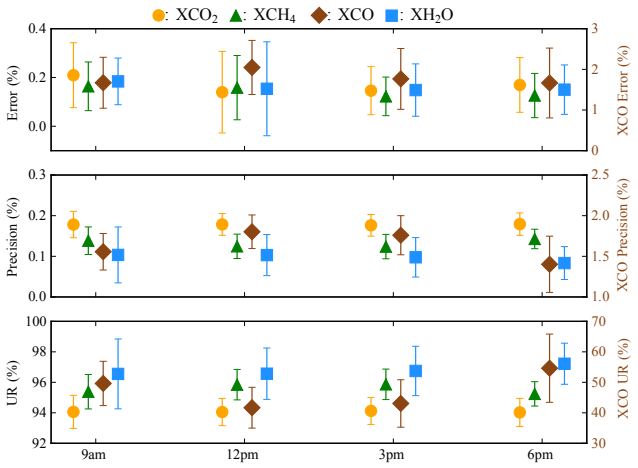

Figure 7. Average retrieval biases, precisions, and uncertainty reductions (URs) for simulated clear-sky retrievals at different times of day (LT). SNR is 300 and spectral resolution is 0.25 cm^{-1}. The a priori is biased 3 % from the truth and has a 3 % uncertainty. The error bars are the standard deviations of retrieval results from all the test cases. Note that the scales for XCO_2, XCH_4, and XH_2O are on the left-hand side whereas those for XCO are on the right-hand side.

For gases that absorb weakly, the absolute value of the single-measurement precision might not be indicative of the retrieval performance. The results here are based on a priori biased 3 % from the truth and have a 3 % uncertainty. As CO absorbs weakly in the chosen spectral bands, the XCO retrievals are relatively more dependent on the a priori. If the a priori were further away from the truth and had a higher uncertainty, the single-measurement precision would get worse accordingly. This makes uncertainty reduction (UR) a more useful quantity as a diagnostic of the observing system.

The retrievals reduce the average uncertainty in XCO_2, XCH_4, XCO, and XH_2O by 94.0, 95.6, 47.2, and 96.8 %, as shown in the third panel of Fig. 7. As CO absorbs weakly, the uncertainty in XCO is only reduced by 47.2 %, which is significantly less than that for the other gases. The weak absorption of CO and the interferences from other strong absorbing gases such as CH_4 and H_2O in the near-infrared are also noted by Buchwitz et al. (2004) and Galli et al. (2012). Our results corroborate Galli et al.'s findings that, due to interferences, the quality of the XCO retrieval is systematically influenced by the shortcomings in CH_4 and H_2O spectroscopy. Nonetheless, the precisions for the simulated retrievals far exceed the measurement requirements discussed in Sect. 1, and thus leave a large margin for other sources of error such as uncertainty in the spectroscopic parameters.

We also notice that the precision and the UR of XCO retrievals tend to follow a diurnal pattern: precision is worse and UR lower at 12 and 3 p.m. than at 9 a.m. and 6 p.m. (LT). This might be due to the different light paths at different times of day. At 12 and 3 p.m. (LT), the solar zenith angles are between 35 to 50°, so incoming sunlight travels through a relatively short path. In contrast, at 9 a.m. and 6 p.m. (LT), the solar zenith angles are between 65 to 85°, so the sunlight traverses a longer light path in the atmosphere, resulting in stronger absorption signals and better precision. In other words, this diurnal pattern in precision might be a feature associated with the viewing geometry from geostationary orbit. Note that these results are based on a constant SNR of 300 and in real retrievals SNR could be kept constant at different times of day if the integration time is adjusted. Whether this diurnal pattern will persist in more simulated or real retrievals warrants more studies in the future.

3.2 Influence of aerosols and clouds

Aerosol and cloud contamination are substantial sources of systematic errors in trace gas retrievals (e.g., Dufour and Bréon, 2003; Houweling et al., 2005; Butz et al., 2011; O'Dell et al., 2012; Merrelli et al., 2015; Zhang et al., 2015). Novel cloud screening algorithms, such as the one designed for the OCO-2 mission, are able to screen out most of the scenes with thick clouds and aerosols. However, even after the pre-screening, some scenes are still contaminated with a small amount of aerosols and ice clouds that have a column-integrated OD less than ~ 0.30 (O'Dell et al., 2012). Following the study just mentioned, we also use OD at 755 nm less than ~ 0.30 as the benchmark for a small amount of aerosols and ice clouds. In these cases, inaccurate retrievals of the optical properties of aerosols and ice clouds will negatively affect the quality of trace gas retrievals.

Here we briefly explore the influence of aerosols and ice clouds on trace gas retrievals and defer detailed investigations to later studies. We add realistic profiles of aerosols and ice clouds to the model atmosphere. It is assumed that the geometric and optical properties of aerosols and ice clouds are known with certainty. Scaling factors for aerosol OD and ice cloud OD are added to the state vector in Eq. (5) and retrievals are repeated for the test cases at 12 p.m. (LT), a time with larger radiance values and higher instrument noise than those at other times of day. Again, the a priori is 3 % biased from the truth and has a 3 % uncertainty. Compared to the clear-sky retrievals in Sect. 3.1, these retrievals are referred to as the all-sky retrievals. The sum of the aerosol and ice cloud ODs is the total particle OD.

Retrieving the ODs of aerosols and clouds from reflected sunlight in near-infrared bands, has been a significant challenge and an active area of scientific research (e.g., Reuter et al., 2010; Herbin et al., 2013). As there are now 11 elements in the state vector (9 elements in Eq. (5) and 2 new elements added), the theoretical upper limit for DoF is 11. However, the real DoF is only about 10.2, mainly due to the lack of information to accurately retrieve the ODs of aerosols and clouds.

Figure 8 shows the retrieval biases, precisions, and URs of the four target species as a function of the total particle OD. Increases in the total particle OD lead to notable in-

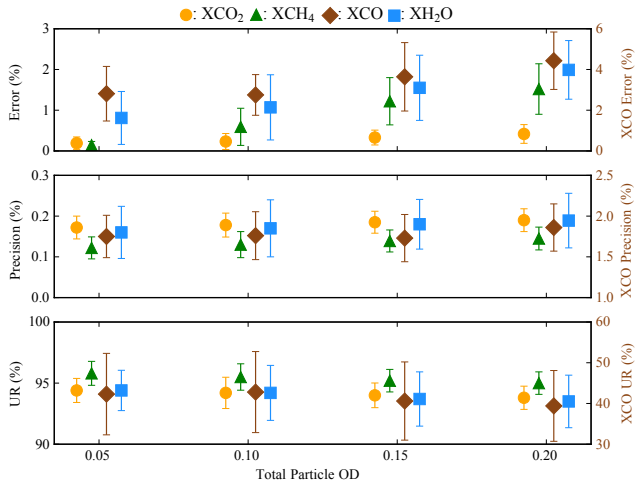

Figure 8. Average retrieval biases, precisions, and uncertainty reductions (UR) for simulated all-sky retrievals as a function of the total particle optical depth (OD) at 755 nm. SNR is 300 and spectral resolution is 0.25 cm^{-1}. The a priori is biased 3 % from the truth and has a 3 % uncertainty. The error bars are the standard deviations of retrieval results from the test cases.

creases in the retrieval biases of all four gases. For XCH_4 and XH_2O, the average retrieval biases increase from < 0.4 % for clear-sky retrievals to 1–3 % for all-sky retrievals. For XCO_2, the biases increase from ∼ 0.2 to ∼ 0.5 %. For XCO, the biases increases from ∼ 1.8 to 2–6 %. Previous studies have obtained similar results. For example, Vidot et al. (2009) conducted simulated retrievals of XCO_2 over liquid water clouds with OCO-2's three spectral bands. They found that the presence of undetected thin cirrus clouds affect all retrieval parameters significantly. These results corroborate the findings of Vidot et al. (2009) that inaccurate retrievals of aerosol and cloud ODs cause substantial biases in XCO_2 retrievals. Through simultaneous retrievals of all four gases, we find that aerosols and clouds cause biases not only in XCO_2 retrievals, but also in all of the trace gas retrievals studied here. Generally, the higher the total particle OD, the worse the retrieval biases are. Spectral measurements from GeoFTS alone do not provide enough information about the optical properties of aerosols and cirrus clouds. This suggests that more effective pre-screening algorithms and better prior knowledge of the aerosol and cloud properties and/or vertical distributions are needed in order to mitigate biases caused by aerosols and clouds.

There are two main causes behind the increase in the retrieval bias. One is the interference between absorption by gases and scattering by aerosols and clouds. The other one is the increase in the forward model error when the total particle OD increases. VLIDORT-16 stream is better at characterizing the multiple light scattering by aerosols and clouds, while 2S-ESS treats light scattering in a more approximate manner. This leads to an increase in the forward model error, and therefore, a corresponding increase in the retrieval bias. These results highlight the need for sophisticated radiative transfer models such as VLIDORT, along with better models to characterize the properties of aerosols and clouds and/or their vertical distributions, so that the forward model error can be minimized for real operational retrievals.

In contrast, the single-measurement precision does not change much when the total particle OD changes. This is expected because, according to Eq. (8), the a posteriori uncertainty and the precision depend on $\mathbf{S}_a$, $\mathbf{S}_e$, and $\mathbf{K}$ only. Changes in total particle OD only affect $\mathbf{S}_e$ and $\mathbf{K}$ slightly, resulting in some minor worsening of the retrieval precision, as illustrated in Fig. 8. These results corroborate the findings of Kuang et al. (2002) using simulations. They also investigated the achievable XCO_2 precisions as a function of the total particle OD and found that, as OD increases from 0.05 to 0.25, the retrieval precision of XCO_2 over land only changes from ∼ 0.5 ppm (∼ 0.13 %) to ∼ 1.0 ppm (∼ 0.26 %). Our results show that the retrieval precisions of all four gases in the absolute sense are only slightly affected by the small amount of aerosol and cloud contamination. Thus, this study provides evidence that the single-measurement precisions for simulated clear-sky and all-sky retrievals meet measurement requirements for accurate flux inversions (Sect. 1).

3.3 Choices of SNR and spectral resolution

The previous sections present retrieval results when SNR and spectral resolution are set at 300 and 0.25 cm^{-1}, respectively. Optimal choices of SNR and spectral resolution can result in better cost–benefit ratio for a geostationary mission. Here we study the effect of varying SNR and spectral resolution on both clear-sky and all-sky retrievals. For simplicity, the two variables are assumed to be independent of each other. To allow easy comparison with retrieval results in Sects. 3.1 and 3.2, the a priori values are same as before. Figure 9 shows the retrieval precision as a function of SNR and spectral resolution, which are set to vary from 50 to 250 and from 0.10 to 0.30 cm^{-1}, respectively. These ranges are chosen so as to cover some possible scenarios for real spaceborne measurements. The total particle OD at 755 nm is zero for clear-sky retrievals and 0.20 for all-sky retrievals. The results shown here are based on one test case at 12 p.m. at Location 1. Other test cases exhibit similar patterns (not shown).

For both clear-sky and all-sky retrievals, the retrieval precision is a strong function of both SNR and spectral resolution. Generally, it increases with higher SNR and finer spectral resolution. Comparing clear-sky and all-sky retrievals, we notice that the precisions for all trace gas retrievals are slightly worse in all-sky retrievals. This is a manifestation of the influence of aerosols and ice clouds, as discussed in Sect. 3.2. In particular, the XCO retrievals are more sensitive to changes in SNR and spectral resolution because of its weak absorption. It is clear that the quality of XCO retrievals is a significant function of both SNR and spectral resolution.

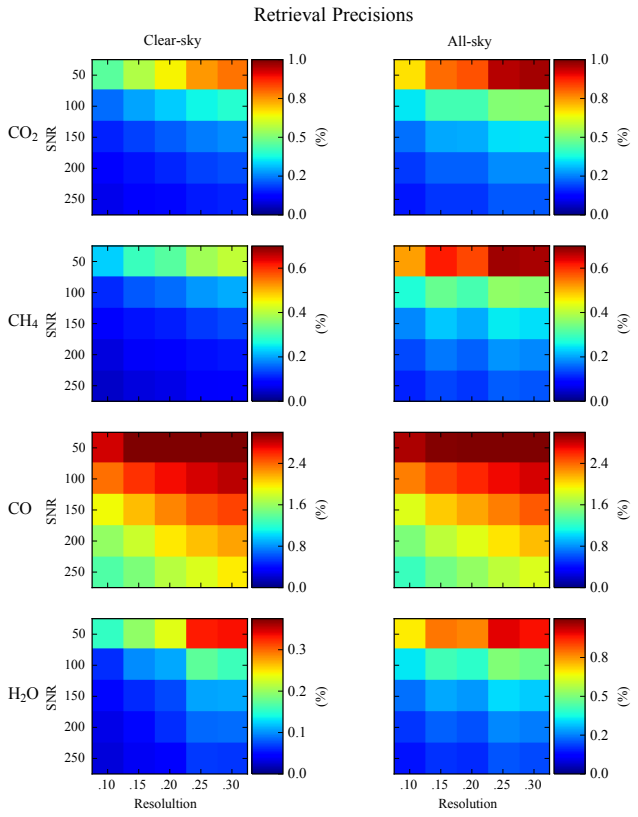

Figure 9. Retrieval precision as a function of SNR and spectral resolution for simulated clear-sky and all-sky retrievals. SNR and spectral resolution are set to vary from 50 to 250 and from 0.10 to 0.30 cm^{-1}, respectively. The a priori is biased 3 % from the truth and has a 3 % uncertainty for all species.

The importance of XCO retrievals for surface flux inversions has been emphasized in Rayner et al. (2014). They investigated the ability of trace gas retrievals to constrain regional GHG emissions and found that XCO retrievals play the most important role in constraining urban emissions at 3 km resolution. Our results show that the choices of SNR and spectral resolution will be of paramount importance for XCO retrievals. This exploratory study could help guide decisions on GeoFTS SNR and spectral resolution, which can result in cost-effective measurement strategies while achieving satisfactory levels of retrieval precisions.

4 Conclusions

This study explores the prospective performance of trace gas retrievals using simulated spectra measured by a Geostationary Fourier Transform Spectrometer (GeoFTS). The major scientific contributions of this study are as follows.

1. We have performed simulated retrievals over a significant range of atmospheric and surface scenarios in clear sky conditions over North America, one potential target for the GeoFTS. We find that, with no uncertainty in spectroscopy, the average retrieval biases and single-measurement precisions are < 0.2 % for XCO_2, XCH_4, and XH_2O, and < 2 % for XCO. These results are based on a priori values with a bias of 3 % and an uncertainty of 3 %.

2. We have briefly explored the influence of aerosols and ice clouds on trace gas retrievals. An increase in the amount of aerosols and ice clouds leads to a notable increase in the retrieval errors and slight worsening of the retrieval precisions. This study provides evidence that the single-measurement precisions for simulated clear-sky and all-sky retrievals meet the requirements for GeoFTS and leave a large margin for other sources of imprecisions in real retrievals.

3. We have studied the effects of varying signal-to-noise ratio (SNR) and spectral resolution on both clear-sky and all-sky retrievals. We find that retrieval precision is a strong function of the two variables. This exploratory study can help guide decisions on GeoFTS SNR and spectral resolution, which can result in cost-effective measurement strategies while achieving satisfactory levels of retrieval precisions.

While this study offers new scientific insights through simulated retrievals, it is worth pointing out that these numerical simulations often provide overoptimistic assessments of the capability of the observing system. This is partly because the instrument noise added to the synthetic data is random, which is unlikely to be the case for real measurements. Furthermore, uncertainty in the spectroscopic parameters, imperfect aerosol/cloud filtering, and various instrument issues will complicate real retrievals. Future studies will focus on how uncertainties in these factors affect the retrieval results.

Acknowledgements. The authors would like to thank Renyu Hu, Pushkar Kopparla, Michael Wong, Le Kuai, Clare (Kam Weng) Wong, and Dejian Fu for helpful discussions. The authors also appreciate technical support from Michael Black and administrative support from Margaret Carlos and Irma Black. Valuable comments and suggestions from two reviewers are greatly appreciated. This research was supported in part by NASA grant NNX13AK34G to the California Institute of Technology, grant P1367828 from the Jet Propulsion Laboratory, and the KISS program at California Institute of Technology.

Edited by: U. Friess

References

Aumann, H. H., Chahine, M. T., Gautier, C., Goldberg, M. D., Kalnay, E., McMillin, L. M., Revercomb, H., Rosenkranz, P. W., Smith, W. L., Staelin, D. H., Strow, L. L., and Susskind, J.: AIRS/AMSU/HSB on the Aqua mission: Design, Science Objectives, Data Products, and Processing Systems, IEEE T. Geosci. Remote, 41, 253–264, doi:10.1109/TGRS.2002.808356, 2003.

Baker, D. F., Bösch, H., Doney, S. C., O'Brien, D., and Schimel, D. S.: Carbon source/sink information provided by column CO_2 measurements from the Orbiting Carbon Observatory, Atmos. Chem. Phys., 10, 4145–4165, doi:10.5194/acp-10-4145-2010, 2010.

Bengtsson, L.: The global atmospheric water cycle, Environ. Res. Lett., 5, 025202, doi:10.1088/1748-9326/5/2/025202, 2010.

Bey, I., Jacob, D. J., Yantosca, R. M., Logan, J. A., Field, B. D., Fiore, A. M., Li, Q., Liu, H. Y., Mickley, L. J., and Schultz, M. G.: Global modeling of tropospheric chemistry with assimilated meteorology: Model description and evaluation, J. Geophys. Res., 106, 23073, doi:10.1029/2001JD000807, 2001.

Bréon, F., O'Brien, D., and Spinhirne, J.: Scattering layer statistics from space borne GLAS observations, Geophys. Res. Lett., 32, L22802, doi:10.1029/2005GL023825, 2005.

Buchwitz, M., de Beek, R., Bramstedt, K., Noël, S., Bovensmann, H., and Burrows, J. P.: Global carbon monoxide as retrieved from SCIAMACHY by WFM-DOAS, Atmos. Chem. Phys., 4, 1945–1960, doi:10.5194/acp-4-1945-2004, 2004.

Buchwitz, M., Schneising, O., Burrows, J. P., Bovensmann, H., Reuter, M., and Notholt, J.: First direct observation of the atmospheric CO_2 year-to-year increase from space, Atmos. Chem. Phys., 7, 4249–4256, doi:10.5194/acp-7-4249-2007, 2007.

Buchwitz, M., Reuter, M., Bovensmann, H., Pillai, D., Heymann, J., Schneising, O., Rozanov, V., Krings, T., Burrows, J. P., Boesch, H., Gerbig, C., Meijer, Y., and Löscher, A.: Carbon Monitoring Satellite (CarbonSat): assessment of atmospheric CO_2 and CH_4 retrieval errors by error parameterization, Atmos. Meas. Tech., 6, 3477–3500, doi:10.5194/amt-6-3477-2013, 2013.

Butz, A., Guerlet, S., Hasekamp, O., Schepers, D., Galli, A., Aben, I., Frankenberg, C., Hartmann, J.-M., Tran, H., Kuze, A., Keppel-Aleks, G., Toon, G., Wunch, D., Wennberg, P., Deutscher, N., Griffith, D., Macatangay, R., Messerschmidt, J., Notholt, J., and Warneke, T.: Toward accurate CO_2 and CH_4 observations from GOSAT, Geophys. Res. Lett., 38, L14812, doi:10.1029/2011GL047888, 2011.

Chahine, M., Barnet, C., Olsen, E. T., Chen, L., and Maddy, E.: On the determination of atmospheric minor gases by the method of vanishing partial derivatives with application to CO_2, Geophys. Res. Lett., 32, L22803, doi:10.1029/2005GL024165, 2005.

Chahine, M. T., Chen, L., Dimotakis, P., Jiang, X., Li, Q., Olsen, E. T., Pagano, T., Randerson, J., and Yung, Y. L.: Satellite remote sounding of mid-tropospheric CO_2, Geophys. Res. Lett., 35, L17807, doi:10.1029/2008GL035022, 2008.

Chevallier, F., Engelen, R. J., and Peylin, P.: The contribution of AIRS data to the estimation of CO_2 sources and sinks, Geophys. Res. Lett., 32, L23801, doi:10.1029/2005GL024229, 2005.

Clough, S. A., Shephard, M. W., Mlawer, E. J., Delamere, J. S., Iacono, M. J., Cady-Pereira, K., Boukabara, S., and Brown, P. D.: Atmospheric radiative transfer modeling: a summary of the AER codes, J. Quant. Spectrosc. Ra. Transf., 91, 233–244, doi:10.1016/j.jqsrt.2004.05.058, 2005.

Crisp, D., Atlas, R. M., Breon, F.-M., Brown, L. R., Burrows, J. P., Ciais, P., Connor, B. J., Doney, S. C., Fung, I. Y., Jacob, D. J., Miller, C. E., O'Brien, D., Pawson, S., Randerson, J. T., Rayner, P., Salawitch, R. J., Sander, S. P., Sen, B., Stephens, G. L., Tans, P. P., Toon, G. C., Wennberg, P. O., Wofsy, S. C., Yung, Y. L., Kuang, Z., Chudasama, B., Sprague, G., Weiss, B., Pollock, R., Kenyon, D., and Schroll, S.: The Orbiting Carbon Observatory (OCO) mission, Adv. Space Res., 34, 700–709, doi:10.1016/j.asr.2003.08.062, 2004.

Crisp, D., Fisher, B. M., O'Dell, C., Frankenberg, C., Basilio, R., Bösch, H., Brown, L. R., Castano, R., Connor, B., Deutscher, N. M., Eldering, A., Griffith, D., Gunson, M., Kuze, A., Mandrake, L., McDuffie, J., Messerschmidt, J., Miller, C. E., Morino, I., Natraj, V., Notholt, J., O'Brien, D. M., Oyafuso, F., Polonsky, I., Robinson, J., Salawitch, R., Sherlock, V., Smyth, M., Suto, H., Taylor, T. E., Thompson, D. R., Wennberg, P. O., Wunch, D., and Yung, Y. L.: The ACOS CO_2 retrieval algorithm – Part II: Global XCO_2 data characterization, Atmos. Meas. Tech., 5, 687–707, doi:10.5194/amt-5-687-2012, 2012.

Connor, B. J., Boesch, H., Toon, G., Sen, B., Miller, C., and Crisp, D.: Orbiting Carbon Observatory: Inverse method and prospective error analysis, J. Geophys. Res.-Atmos., 113, D05305, doi:10.1029/2006JD008336, 2008.

Dufour, E. and Bréon, F.-M.: Spaceborne Estimate of Atmospheric CO_2 Column by Use of the Differential Absorption Method: Error Analysis, Appl. Opt., 42, 3595, doi:10.1364/AO.42.003595, 2003.

Fu, D., Pongetti, T. J., Blavier, J.-F. L., Crawford, T. J., Manatt, K. S., Toon, G. C., Wong, K. W., and Sander, S. P.: Near-infrared remote sensing of Los Angeles trace gas distributions from a mountaintop site, Atmos. Meas. Tech., 7, 713–729, doi:10.5194/amt-7-713-2014, 2014.

Galli, A., Butz, A., Scheepmaker, R. A., Hasekamp, O., Landgraf, J., Tol, P., Wunch, D., Deutscher, N. M., Toon, G. C., Wennberg, P. O., Griffith, D. W. T., and Aben, I.: CH_4, CO, and H_2O spectroscopy for the Sentinel-5 Precursor mission: an assessment with the Total Carbon Column Observing Network measurements, Atmos. Meas. Tech., 5, 1387–1398, doi:10.5194/amt-5-1387-2012, 2012.

Herbin, H., Labonnote, L. C., and Dubuisson, P.: Multispectral information from TANSO-FTS instrument – Part 2: Application to aerosol effect on greenhouse gas retrievals, Atmos. Meas. Tech., 6, 3313–3323, doi:10.5194/amt-6-3313-2013, 2013.

Heymsfield, A., Bansemer, A., Field, P., Durden, S., Stith, J., Dye, J., Hall, W., and Grainger, C.: Observations and Parameterizations of Particle Size Distributions in Deep Tropical Cirrus and Stratiform Precipitating Clouds: Results from In Situ Observations in TRMM Field Campaigns, J. Atmos. Sci., 59, 3457–3491, 2002.

Houghton, R. A.: Balancing the Global Carbon Budget, Annu. Rev. Earth Planet. Sci., 35, 313–347, doi:10.1146/annurev.earth.35.031306.140057, 2007.

Houweling, S., Hartmann, W., Aben, I., Schrijver, H., Skidmore, J., Roelofs, G.-J., and Breon, F.-M.: Evidence of systematic errors in SCIAMACHY-observed CO_2 due to aerosols, Atmos. Chem. Phys., 5, 3003–3013, doi:10.5194/acp-5-3003-2005, 2005.

Hungershoefer, K., Breon, F.-M., Peylin, P., Chevallier, F., Rayner, P., Klonecki, A., Houweling, S., and Marshall, J.: Evaluation of various observing systems for the global monitoring of

CO_2 surface fluxes, Atmos. Chem. Phys., 10, 10503–10520, doi:10.5194/acp-10-10503-2010, 2010.

IPCC: Climate Change 2013: The physical science basis. Contribution of working group I to the fifth assessment report of the Intergovernmental Panel on Climate Change, edited by: Stocker, T. F., Qin, D., Plattner, G.-K., Tignor, M., Allen, S. K., Boschung, J., Nauels, A., Xia, Y., Bex, V., and Midgley, P. M., Cambridge University Press, Cambridge, United Kingdom and New York, NY, USA, 1535 pp., 2013.

Jacob, F., Petitcolin, F., Schmugge, T., Vermote, É., French, A., and Ogawa, K.: Comparison of land surface emissivity and radiometric temperature derived from MODIS and ASTER sensors, Remote Sens. Environ., 90, 137–152, doi:10.1016/j.rse.2003.11.015, 2004.

Key, R., Sander, S., Eldering, A., Miller, C., Frankenberg, C., Natraj, V., Rider, D., Blavier, J., Bekker, D., and Wu, Y. H.: The Geostationary Carbon Process Mapper, in 2012 IEEE Aerospace Conference, 1–16, IEEE, 2012.

Kuai, L., Natraj, V., Shia, R.-L., Miller, C., and Yung, Y. L.: Channel selection using information content analysis: A case study of CO_2 retrieval from near infrared measurements, J. Quant. Spectrosc. Ra. Transf., 111, 1296–1304, doi:10.1016/j.jqsrt.2010.02.011, 2010.

Kuang, Z., Margolis, J., Toon, G., Crisp, D., and Yung, Y.: Spaceborne measurements of atmospheric CO_2 by high-resolution NIR spectrometry of reflected sunlight: An introductory study, Geophys. Res. Lett., 29, 11-1–11-4, doi:10.1029/2001GL014298, 2002.

Le Quéré, C., Raupach, M. R., Canadell, J. G., Marland, G., Bopp, L., Ciais, P., Conway, T. J., Doney, S. C., Feely, R. A., Foster, P., Friedlingstein, P., Gurney, K., Houghton, R. A., House, J. I., Huntingford, C., Levy, P. E., Lomas, M. R., Majkut, J., Metzl, N., Ometto, J. P., Peters, G. P., Prentice, I. C., Randerson, J. T., Running, S. W., Sarmiento, J. L., Schuster, U., Sitch, S., Takahashi, T., Viovy, N., van der Werf, G. R., and Woodward, F. I.: Trends in the sources and sinks of carbon dioxide, Nat. Geosci., 2, 831–836, doi:10.1038/ngeo689, 2009.

Le Quéré, C., Peters, G. P., Andres, R. J., Andrew, R. M., Boden, T. A., Ciais, P., Friedlingstein, P., Houghton, R. A., Marland, G., Moriarty, R., Sitch, S., Tans, P., Arneth, A., Arvanitis, A., Bakker, D. C. E., Bopp, L., Canadell, J. G., Chini, L. P., Doney, S. C., Harper, A., Harris, I., House, J. I., Jain, A. K., Jones, S. D., Kato, E., Keeling, R. F., Klein Goldewijk, K., Körtzinger, A., Koven, C., Lefèvre, N., Maignan, F., Omar, A., Ono, T., Park, G. H., Pfeil, B., Poulter, B., Raupach, M. R., Regnier, P., Rödenbeck, C., Saito, S., Schwinger, J., Segschneider, J., Stocker, B. D., Takahashi, T., Tilbrook, B., van Heuven, S., Viovy, N., Wanninkhof, R., Wiltshire, A., and Zaehle, S.: Global carbon budget 2013, Earth Syst. Sci. Data, 6, 235–263, doi:10.5194/essd-6-235-2014, 2014.

Levenberg, K.: A method for the solution of certain problems in least squares, Quart. Applied Math., 2, 164–168, 1944.

Marquardt, D. W.: An Algorithm for Least-Squares Estimation of Nonlinear Parameters, J. Soc. Indust. Appl. Math., 11, 431–441, doi:10.1137/0111030, 1963.

Merrelli, A., Bennartz, R., O'Dell, C. W., and Taylor, T. E.: Estimating bias in the OCO-2 retrieval algorithm caused by 3-D radiation scattering from unresolved boundary layer clouds, Atmos. Meas. Tech., 8, 1641–1656, doi:10.5194/amt-8-1641-2015, 2015.

Nassar, R., Jones, D. B. A., Kulawik, S. S., Worden, J. R., Bowman, K. W., Andres, R. J., Suntharalingam, P., Chen, J. M., Brenninkmeijer, C. A. M., Schuck, T. J., Conway, T. J., and Worthy, D. E.: Inverse modeling of CO_2 sources and sinks using satellite observations of CO_2 from TES and surface flask measurements, Atmos. Chem. Phys., 11, 6029–6047, doi:10.5194/acp-11-6029-2011, 2011.

Natraj, V.: A review of fast radiative transfer techniques, in: Light Scattering Reviews 8, edited by: Kokhanovsky, A. A., 475–504, Springer Berlin Heidelberg, Berlin, Heidelberg, 2013.

Newman, S., Jeong, S., Fischer, M. L., Xu, X., Haman, C. L., Lefer, B., Alvarez, S., Rappenglueck, B., Kort, E. A., Andrews, A. E., Peischl, J., Gurney, K. R., Miller, C. E., and Yung, Y. L.: Diurnal tracking of anthropogenic CO_2 emissions in the Los Angeles basin megacity during spring 2010, Atmos. Chem. Phys., 13, 4359–4372, doi:10.5194/acp-13-4359-2013, 2013.

O'Dell, C. W., Connor, B., Bösch, H., O'Brien, D., Frankenberg, C., Castano, R., Christi, M., Eldering, D., Fisher, B., Gunson, M., McDuffie, J., Miller, C. E., Natraj, V., Oyafuso, F., Polonsky, I., Smyth, M., Taylor, T., Toon, G. C., Wennberg, P. O., and Wunch, D.: The ACOS CO_2 retrieval algorithm – Part 1: Description and validation against synthetic observations, Atmos. Meas. Tech., 5, 99–121, doi:10.5194/amt-5-99-2012, 2012.

Polonsky, I. N., O'Brien, D. M., Kumer, J. B., O'Dell, C. W., and the geoCARB Team: Performance of a geostationary mission, geoCARB, to measure CO_2, CH_4 and CO column-averaged concentrations, Atmos. Meas. Tech., 7, 959–981, doi:10.5194/amt-7-959-2014, 2014.

Rayner, P. J. and O'Brien, D. M.: The utility of remotely sensed CO_2 concentration data in surface source inversions, Geophys. Res. Lett., 28, 175–178, doi:10.1029/2000GL011912, 2001.

Rayner, P. J., Utembe, S. R., and Crowell, S.: Constraining regional greenhouse gas emissions using geostationary concentration measurements: a theoretical study, Atmos. Meas. Tech., 7, 3285–3293, doi:10.5194/amt-7-3285-2014, 2014.

Reuter, M., Buchwitz, M., Schneising, O., Heymann, J., Bovensmann, H., and Burrows, J. P.: A method for improved SCIAMACHY CO_2 retrieval in the presence of optically thin clouds, Atmos. Meas. Tech., 3, 209–232, doi:10.5194/amt-3-209-2010, 2010.

Rodgers, C. D.: Information content and optimisation of high spectral resolution remote measurements, Adv. Space Res., 21, 361–367, doi:10.1016/S0273-1177(97)00915-0, 1998.

Rodgers, C. D.: Inverse Methods for Atmospheric Sounding: Theory and Practice, World Scientific, Singapore, 2000.

Rothman, L. S., Gordon, I. E., Barbe, A., Benner, D. C., Bernath, P. F., Birk, M., Boudon, V., Brown, L. R., Campargue, A., Champion, J.-P., Chance, K., Coudert, L. H., Dana, V., Devi, V. M., Fally, S., Flaud, J.-M., Gamache, R. R., Goldman, A., Jacquemart, D., Kleiner, I., Lacome, N., Lafferty, W. J., Mandin, J.-Y., Massie, S. T., Mikhailenko, S. N., Miller, C. E., Moazzen-Ahmadi, N., Naumenko, O. V., Nikitin, A. V., Orphal, J., Perevalov, V. I., Perrin, A., Predoi-Cross, A., Rinsland, C. P., Rotger, M., Šimečková, M., Smith, M. A. H., Sung, K., Tashkun, S. A., Tennyson, J., Toth, R. A., Vandaele, A. C., and Vander Auwera, J.: The HITRAN 2008 molecular spectroscopic database, J. Quant. Spectrosc. Ra. Transf., 110, 533–572, doi:10.1016/j.jqsrt.2009.02.013, 2009.

Schimel, D. S., House, J. I., Hibbard, K. A., Bousquet, P., Ciais, P., Peylin, P., Braswell, B. H., Apps, M. J., Baker, D., Bondeau, A., Canadell, J., Churkina, G., Cramer, W., Denning, A. S., Field, C. B., Friedlingstein, P., Goodale, C., Heimann, M., Houghton, R. A., Melillo, J. M., Moore III, B., Murdiyarso, D., Noble, I., Pacala, S. W., Prentice, I. C., Raupach, M. R., Rayner, P. J., Scholes, R. J., Steffen, W. L., and Wirth, C.: Recent patterns and mechanisms of carbon exchange by terrestrial ecosystems, Nature, 414, 169–172, 2001.

Schneising, O., Buchwitz, M., Reuter, M., Heymann, J., Bovensmann, H., and Burrows, J. P.: Long-term analysis of carbon dioxide and methane column-averaged mole fractions retrieved from SCIAMACHY, Atmos. Chem. Phys., 11, 2863–2880, doi:10.5194/acp-11-2863-2011, 2011.

Schrijver, H., Gloudemans, A. M. S., Frankenberg, C., and Aben, I.: Water vapour total columns from SCIAMACHY spectra in the 2.36 µm window, Atmos. Meas. Tech., 2, 561–571, doi:10.5194/amt-2-561-2009, 2009.

Spurr, R. J. D.: VLIDORT: A linearized pseudo-spherical vector discrete ordinate radiative transfer code for forward model and retrieval studies in multilayer multiple scattering media, J. Quant. Spectrosc. Ra. Transf., 102, 316–342, doi:10.1016/j.jqsrt.2006.05.005, 2006.

Spurr, R. and Natraj, V.: A linearized two-stream radiative transfer code for fast approximation of multiple-scatter fields, J. Quant. Spectrosc. Ra. Transf., 112, 2630–2637, doi:10.1016/j.jqsrt.2011.06.014, 2011.

Vidot, J., Bennartz, R., O'Dell, C. W., Preusker, R., Lindstrot, R., and Heidinger, A. K.: CO_2 Retrieval over Clouds from the OCO Mission: Model Simulations and Error Analysis, J. Atmos. Ocean. Technol., 26, 1090–1104, doi:10.1175/2009JTECHA1200.1, 2009.

Wecht, K. J., Jacob, D. J., Sulprizio, M. P., Santoni, G. W., Wofsy, S. C., Parker, R., Bösch, H., and Worden, J.: Spatially resolving methane emissions in California: constraints from the CalNex aircraft campaign and from present (GOSAT, TES) and future (TROPOMI, geostationary) satellite observations, Atmos. Chem. Phys., 14, 8173–8184, doi:10.5194/acp-14-8173-2014, 2014.

Winker, D. M., Pelon, J., Coakley, J. A., Ackerman, S. A., Charlson, R. J., Colarco, P. R., Flamant, P., Fu, Q., Hoff, R. M., Kittaka, C., Kubar, T. L., Le Treut, H., McCormick, M. P., Mégie, G., Poole, L., Powell, K., Trepte, C., Vaughan, M. A., and Wielicki, B. A.: The Calipso Mission: A Global 3D View of Aerosols and Clouds, B. Am. Meteorol. Soc., 91, 1211–1229, doi:10.1175/2010BAMS3009.1, 2010.

Wong, K. W., Fu, D., Pongetti, T. J., Newman, S., Kort, E. A., Duren, R., Hsu, Y.-K., Miller, C. E., Yung, Y. L., and Sander, S. P.: Mapping $CH_4 : CO_2$ ratios in Los Angeles with CLARS-FTS from Mount Wilson, California, Atmos. Chem. Phys., 15, 241–252, doi:10.5194/acp-15-241-2015, 2015.

Woods, T. N., Chamberlin, P. C., Harder, J. W., Hock, R. A., Snow, M., Eparvier, F. G., Fontenla, J., McClintock, W. E., and Richard, E. C.: Solar Irradiance Reference Spectra (SIRS) for the 2008 Whole Heliosphere Interval (WHI), Geophys. Res. Lett., 36, L01101, doi:10.1029/2008GL036373, 2009.

Wu, L., Bocquet, M., Lauvaux, T., Chevallier, F., Rayner, P., and Davis, K.: Optimal representation of source-sink fluxes for mesoscale carbon dioxide inversion with synthetic data, J. Geophys. Res.-Atmos., 116, D21304, doi:10.1029/2011JD016198, 2011.

Wunch, D., Wennberg, P. O., Toon, G. C., Connor, B. J., Fisher, B., Osterman, G. B., Frankenberg, C., Mandrake, L., O'Dell, C., Ahonen, P., Biraud, S. C., Castano, R., Cressie, N., Crisp, D., Deutscher, N. M., Eldering, A., Fisher, M. L., Griffith, D. W. T., Gunson, M., Heikkinen, P., Keppel-Aleks, G., Kyrö, E., Lindenmaier, R., Macatangay, R., Mendonca, J., Messerschmidt, J., Miller, C. E., Morino, I., Notholt, J., Oyafuso, F. A., Rettinger, M., Robinson, J., Roehl, C. M., Salawitch, R. J., Sherlock, V., Strong, K., Sussmann, R., Tanaka, T., Thompson, D. R., Uchino, O., Warneke, T., and Wofsy, S. C.: A method for evaluating bias in global measurements of CO_2 total columns from space, Atmos. Chem. Phys., 11, 12317–12337, doi:10.5194/acp-11-12317-2011, 2011.

Xiong, X., Barnet, C., Maddy, E., Sweeney, C., Liu, X., Zhou, L., and Goldberg, M.: Characterization and validation of methane products from the Atmospheric Infrared Sounder (AIRS), J. Geophys. Res., 113, G00A01, doi:10.1029/2007JG000500, 2008.

Yokota, T., Yoshida, Y., Eguchi, N., Ota, Y., Tanaka, T., Watanabe, H., and Maksyutov, S.: Global Concentrations of CO_2 and CH_4 Retrieved from GOSAT: First Preliminary Results, SOLA, 5, 160–163, doi:10.2151/sola.2009-041, 2009.

Yoshida, Y., Ota, Y., Eguchi, N., Kikuchi, N., Nobuta, K., Tran, H., Morino, I., and Yokota, T.: Retrieval algorithm for CO_2 and CH_4 column abundances from short-wavelength infrared spectral observations by the Greenhouse gases observing satellite, Atmos. Meas. Tech., 4, 717–734, doi:10.5194/amt-4-717-2011, 2011.

Zhang, Q., Natraj, V., Li, K., Shia, R., Fu, D., Pongetti, T., Sander, S. P., and Yung, Y. L.: Influence of aerosol scattering on the retrieval of CO_2 mixing ratios: a case study using measurements from the California Laboratory for Atmospheric Remote Sensing (CLARS), J. Geophys. Res.-Atmos., 120, 7205–7218, doi:10.1002/2015JD023499, 2015.